

RESEARCH ARTICLE

Open Access



Infection risk assessment due to contaminant leakage in biological laboratories in different scenarios - the case of COVID-19 virus

Hu Gao^{1,2}, Jing Liu^{1,2*}, Liping Qiu³, Weiwei Wu³ and Weixin Qian^{1,2}

Abstract

Biosafety laboratories are specialized in handling dangerous microorganisms, but there are cases where contaminants are leaked due to improper handling and other reasons. Therefore, an in-depth understanding of the pattern of infection after a laboratory spill can help laboratory personnel get out of danger as soon as possible and avoid the occurrence of infection events. In this paper, we take the COVID-19 virus outbreak in recent years as an example to explore the probability of infection of laboratory personnel under different circumstances. The study used computational fluid dynamics (CFD) to predict the change of contaminant concentration over time in a typical laboratory, and then analyzed the relationship between contaminant concentration and infection probability by using a metrological response model, and calculated the infection probability of indoor personnel over time in the presence or absence of obstacles in the laboratory and the different locations of contaminant leakage, respectively. The results showed that the probability of personnel infection remained basically stable after 8 min of contaminant leakage; at the same time, the probability of infection was higher when the contaminant source was located below the exhaust vent than in other locations; and the probability of illness was lower in laboratories with obstacles than in laboratories without obstacles under the same conditions. This finding is helpful for laboratory layout design.

Keywords Dose-response, Biosafety laboratories, Risk assessment, COVID-19, CFD

1 Introduction

Biosafety Laboratories (BSLs) are the primary protective measure against highly infectious microorganisms and toxins and are designed to protect staff and the environment from infectious substances. Indeed despite the

relatively sophisticated technical systems and measures in place in current biosafety laboratories, laboratory personnel are always at risk of being infected when handling microorganisms.

Since the world's first laboratory infection was reported in France in 1893 (Lippi et al., 2020), similar incidents have occurred from time to time, raising concerns about laboratory safety. For example, in 2003, a microbiology student in Singapore was admitted to the hospital with fever and was eventually confirmed to be infected with SARS coronavirus (SARS-CoV) (Lim et al., 2004); and in 2014, a case of dengue virus infection acquired by a laboratory worker was reported in South Korea (Lee et al., 2016). A series of laboratory infections have raised concerns about the incidence of laboratory infections. Data

*Correspondence:

Jing Liu

liujinghit@hit.edu.cn

¹ School of Architecture, Harbin Institute of Technology, Harbin 150090, China

² Key Laboratory of Cold Region Urban and Rural Human Settlement Environment Science and Technology, Ministry of Industry and Information Technology, Harbin 150090, China

³ China Academy of Building Research, Beijing 100039, People's Republic of China



© The Author(s) 2024. **Open Access** This article is licensed under a Creative Commons Attribution 4.0 International License, which permits use, sharing, adaptation, distribution and reproduction in any medium or format, as long as you give appropriate credit to the original author(s) and the source, provide a link to the Creative Commons licence, and indicate if changes were made. The images or other third party material in this article are included in the article's Creative Commons licence, unless indicated otherwise in a credit line to the material. If material is not included in the article's Creative Commons licence and your intended use is not permitted by statutory regulation or exceeds the permitted use, you will need to obtain permission directly from the copyright holder. To view a copy of this licence, visit <http://creativecommons.org/licenses/by/4.0/>.

summarizing the past 219 laboratory infection incidents showed that 73% of laboratory-acquired infections were caused by aerosol spills (Pedrosa & Cardoso, 2011).

The 2019 outbreak of a novel coronavirus, COVID-19, in Wuhan, China, was the third coronavirus pandemic in the last 20 years, following respiratory diseases such as Severe Acute Respiratory Syndrome (SARS) and Middle East Respiratory Syndrome (MERS) (Lippi et al., 2020), which the World Health Organization named SARS-CoV-2, and classified as a category 3 organism of risk using a level 2 or level 3 biosafety laboratories (BSL-2-3) for handling (Naeem et al., 2022). There is evidence that the novel coronavirus COVID-19 can be transmitted via aerosols (Wu et al., 2020). Therefore, understanding the spatial distribution of SARS-CoV-2 viruses is important for laboratory design and management. CFD numerical simulations are commonly used to predict the distribution of flow fields and particulate matter. In a previous study, Liu et al. used numerical simulation to predict the migration and deposition behaviours of aerosol particulate matter in BSL-3 (Liu et al., 2020a), and investigated the bioaerosol removal rate and spatial suspension rate over time for both the presence and absence of equipment obstacles in the room (Liu et al., 2020b). On the other hand, bioaerosol concentration indirectly reflects the magnitude of infection probability, but there is no linear relationship between these two parameters. Huang et al. evaluated the risk of infection during an outbreak of COVID-19 in an auditorium in Hunan Province, China, using the Wells-Riley model, and the results showed that increasing air ventilation or supplying outdoor air alone could not effectively reduce the risk of infection, and that the protective effect of maintaining social distance was limited. The results showed that increasing air ventilation or supplying outdoor air alone could not effectively reduce the risk of infection, and the protective effect of maintaining social distance was limited, but replacement ventilation and wearing masks could effectively reduce the risk of infection (Huang et al., 2022). Qian et al. combined the Wells-Riley model with CFD to analyze the spatial distribution of the risk of SARS virus infection in hospital wards, and the predicted results were consistent with the observed spatial distribution of infected medical students and inpatients (Qian et al., 2009). Yin et al. used CFD to simulate the airflow pattern and the dispersion of infectious particles in the cabin of an airplane, and then used a dose-response model to assess the risk of infection in the presence of a range of infectious agents at a range of intensity values. Values of infectious agent intensities, and then used dose-response modeling to assess the infection risk of passengers (Yin et al., 2012).

The biosafety laboratories, as the most frequently exposed to viruses, need to maintain the indoor

cleanliness requirements at all times and minimize the incidents of personnel infection after virus leakage occurs. Therefore, it is of great significance to rationally plan the laboratory layout. In this paper, the influence of contaminant leakage location and indoor layout on the probability of personnel infection under the cleanliness requirements of biosafety laboratories is investigated by using Computational Fluid Dynamics (CFD) technology combined with dose-response modeling, which provides a strong theoretical support for laboratory design and safety management.

The article makes specific contributions in the following manner: In the second chapter, an introduction to the aerosol model and the Dose-Response model is provided, accompanied by a succinct overview of the Computational Fluid Dynamics (CFD) solving settings utilized in the study. Chapter three delves into the dynamic changes in aerosol distribution over time. It systematically analyzes the impact of various factors, such as different aerosol leakage points and the presence of obstacles, on aerosol release. The fourth chapter functions as a conclusive summary of the work presented in the paper.

2 Materials/methods

2.1 Laboratory models

The experiment was conducted in a tertiary biology laboratory with dimensions of 7.95 m in length, 4.15 m in width, and 2.7 m in height. The laboratory is equipped with two supply air outlets and three exhaust air outlets. Two exhaust outlets are located in the ceiling, while one provides supplemental exhaust air for the biosafety cabinet. The supply air is introduced through a 0.63 m × 0.63 m square diffuser with a velocity set at 0.57 m/s. The exhaust air is extracted through a 0.483 m × 0.483 m square diffuser. The biosafety cabinet is supplied with air through a 1 m × 0.64 m inlet with an air velocity of 0.35 m/s.

The background of the experiment is a tertiary biology laboratory with dimensions of 7.95 m in length, 4.15 m in width, and 2.7 m in height. The laboratory is equipped with two supply air outlets and three exhaust air outlets. Two exhaust outlets are located in the ceiling, while one provides supplemental exhaust air for the biosafety cabinet. The supply air is introduced through a 0.63 m × 0.63 m square diffuser with a velocity set at 0.57 m/s. The exhaust air is extracted through a 0.483 m × 0.483 m square diffuser. The biosafety cabinet is supplied with air through a 1 m × 0.64 m inlet with an air velocity of 0.35 m/s. The room has two supply air inlets and three exhaust air outlets, two of which are located in the ceiling and the other one provides supplementary exhaust air to the biosafety cabinet. The room model is comparable to the actual size

of the laboratory, which includes an A2 biosafety cabinet, a liquid nitrogen tank, a carbon dioxide incubator, and an incubator, and contains two mannequins in the room. In the modeling, the CO₂ incubator, the incubator, the bio-centrifuge, the nucleic acid extractor, the microscope, the transfer window, and the refrigerator were modeled in a simplified structure to simplify the numerical calculations and subsequent flow field analysis. Figure 1 provides a schematic representation of the constructed model. In Fig. 1a, the physical model is depicted with obstacles placed transversely, whereas Fig. 1b illustrates the physical model with obstacles positioned longitudinally. The conditions in Fig. 1b mirror those in Fig. 1a, with the sole distinction lying in

the variation of obstacle placement. Since experimental activities that generate aerosol leakage (including inoculation, aspiration, injection, centrifugation, dissection, etc.) generally occur on the operating table, the location of the contaminant release source is usually set on the operating table. In order to compare the effect of airflow on the diffusion of the contaminant source, this paper uses three locations to place the contaminant source, which are placed on two tables and directly under the air outlet. Meanwhile, in order to analyse the effect of obstacles in the room on the diffusion of pollutants, an additional room without any experimental equipment is set up as a comparison experiment.

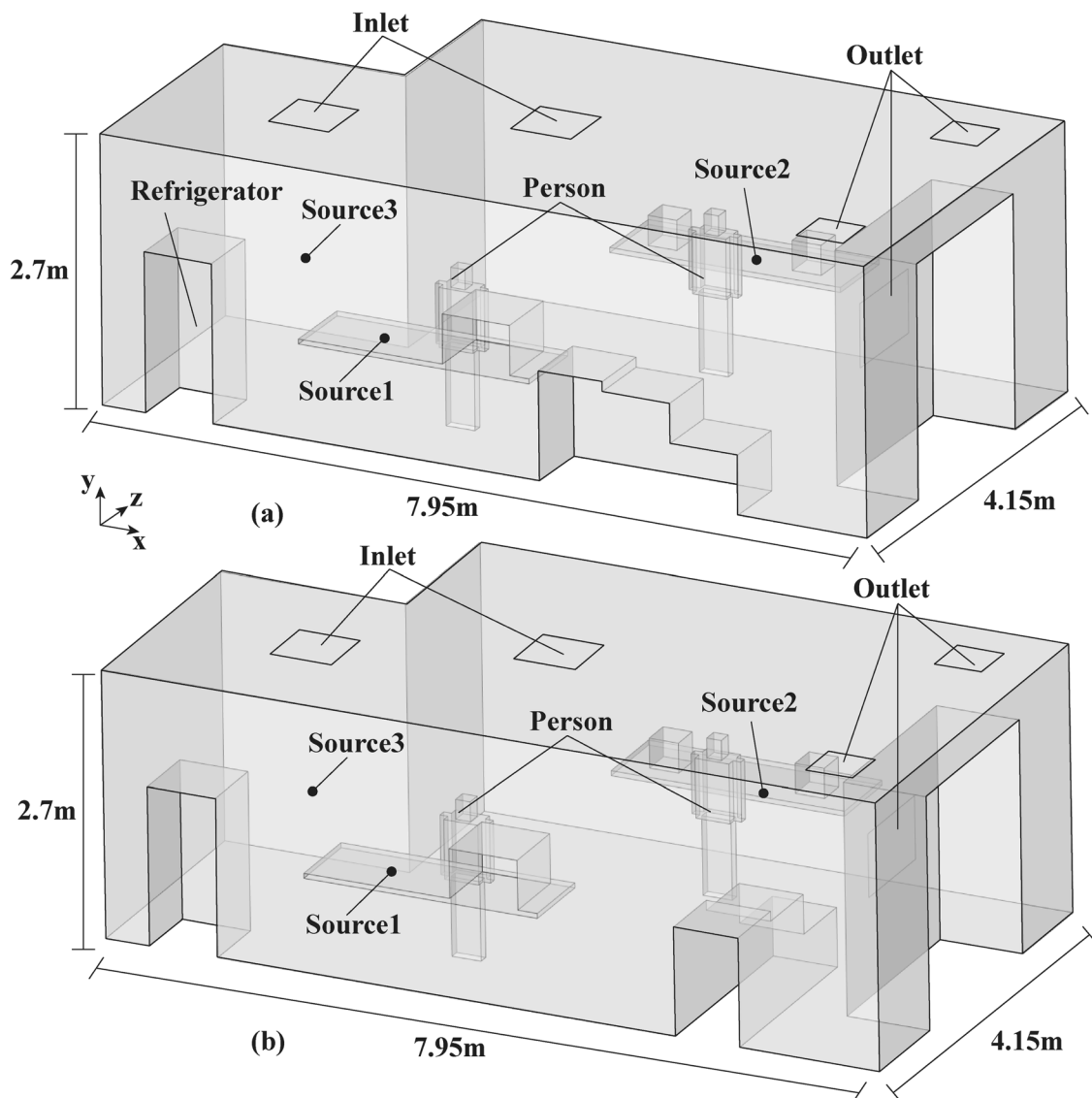


Fig. 1 Schematic diagram of the laboratory model, **a** model 1; **b** model 2

2.2 Aerosol models

Given that viruses cannot persist in the air independently for extended periods, it is assumed that the SARS-CoV-2 virus exists in association with aerosols when leaked. Studies indicate that the size of aerosols in the air is not constant. Aerosols undergo the process of evaporation during propagation, resulting in a gradual decrease in size. However, owing to the presence of solutes, complete evaporation does not occur. Instead, the aerosol progressively contracts into a small droplet nucleus.

The relationship between the final aerosol size and the initial state size is as follows:

$$d_{pc} = \left(\frac{\Phi_i}{\Psi_{max}} \right)^{1/3} d_{p0} \tag{1}$$

where Φ_i is the proportion of solids in the initial state, which is 1.8% according to Nicas et al. (2005); and Ψ_{max} is the maximum solid volume ratio in the droplet nucleus, which is about 0.5236. At room temperature, a 100 μm aerosol can be evaporated to the droplet-nucleus state in tens of seconds (Fig. 2).

Therefore, in this paper, we assume that the aerosol containing the virus is a spherical particle with a diameter of $1\text{e-}5$ m. And since the main component of the aerosol is water, the density of the aerosol is assumed to be 1000 kg/m^3 .

2.3 Numerical modeling of virus spread and propagation

CFD stands out as one of the most potent tools for investigating fluid flow and pollutant dispersion. This paper utilizes Ansys Fluent 2022 R1, a widely used commercial CFD software, for numerical simulations. Specifically, for incompressible gases, the SST turbulence model has demonstrated promising applications in confined spaces (Yu & Thé, 2016). To ensure both stability and precision in numerical calculations, the second-order windward format is adopted, and the SIMPLE algorithm is employed for airflow field calculations. The detailed boundary conditions are outlined in Table 1:

Table 1 Boundary conditions

Parameters	Conditions
Mesh number	0.23 million
Mesh type	Regular hexahedral mesh
Turbulence model	SST k-w model
Boundary	
Inlet	Velocity inlet: 0.7 m/s
Outlet	Pressure outlet: -25 Pa
Other walls	No-slip boundary
Solution methods scheme	Coupled
Discretization	Quick

Due to significant wind speed gradients at the supply and return air outlets, an assessment of the airflow velocity at the diffuser locations is necessary. The mean absolute percentage error (MAPE) metric is employed to evaluate the discrepancy between experimental data and simulation results, expressed by the following equation:

$$MAPE(y, \tilde{y}) = \frac{1}{n} \sum_{i=1}^n \left| \frac{y_i - \tilde{y}_i}{y_i} \right|$$

Comparisons between simulated results and measured data are illustrated in Fig. 3, with a mean absolute percentage error (MAPE) for velocity calculated at 16%, indicating a commendable level of consistency. Consequently, the mathematical model is validated, rendering it suitable for further numerical simulation studies.

For aerosol diffusion in air, particles are tracked using the Lagrangian method and the Discrete Random Wandering (DRW) model is used to take into account the effect of random turbulence on particle diffusion. The Lagrangian method places a set of particles inside a packet and tracks these particles by solving the equations of motion of the packet. The equations of motion can be written in the following:

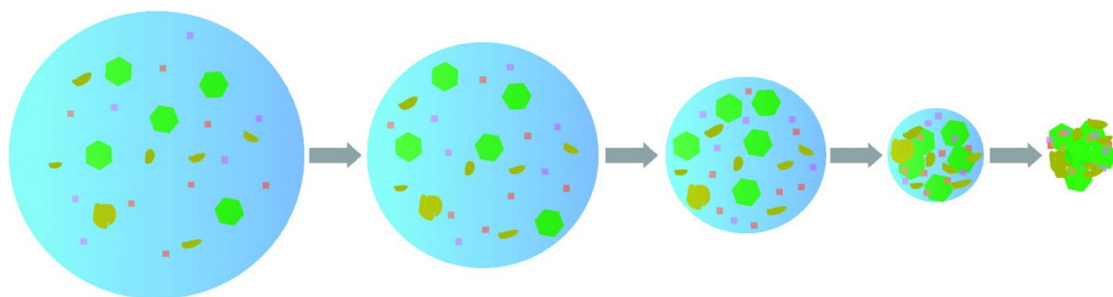


Fig. 2 Evaporation of a droplet (left) into a droplet nucleus (right) (image credit: (Verreault et al., 2008))

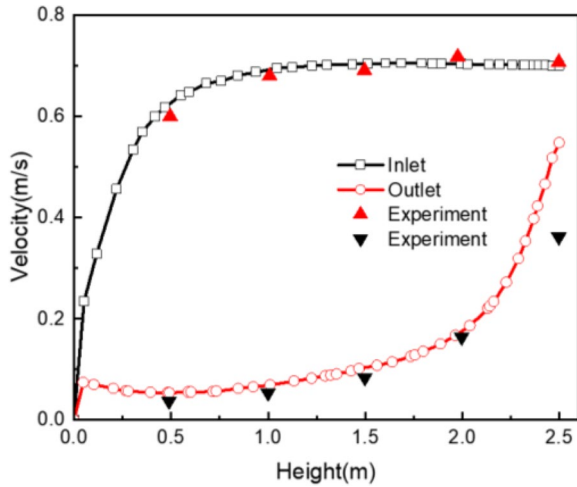


Fig. 3 Comparison of simulated airflow field velocities with measured data. (Experimental data from reference: Liu et al., 2020a)

$$m_p \frac{d\vec{u}_p}{dt} = m_p \frac{\vec{u} - \vec{u}_p}{\tau_r} + m_p \frac{\vec{g}(\rho_p - \rho)}{\rho_p} + \vec{F} \quad (2)$$

where m_p is the mass of the particle packet, u and u_p are the velocities of the continuous and discrete terms, respectively, ρ and ρ_p are the densities of the continuous and discrete terms, respectively, and the first term on the right-hand side of the equation represents the drag force. The third term to the right of the equal sign in Eq. (2) denotes the additional forces exerted on the particle, depending on the flow conditions and particle properties. These forces include pressure gradient forces due to non-constant flow, virtual mass forces, Brownian forces, thermophoretic forces, Bassett forces, and Saffman lift forces (Zhao et al., 2004). These forces were analyzed in terms of magnitude, and some of them are so small as to be negligible. Based on previous literature (Watanabe et al., 2010), only Brownian and Saffman lift forces were finally considered in this study. It is also assumed that the proportion of aerosols in the air is small enough to have a negligible effect on the airflow and that the simulation uses unidirectional coupling, an assumption that is reasonable in laboratories with high cleanliness requirements.

2.4 Dose–response model

The Dose-Response model is a mathematical tool that examines the correlation between the amount of a substance (dose) and the corresponding biological reaction (response) in an organism. It is commonly utilized to analyze the impact of drugs, toxins, radiation, and similar factors. Watanabe proposed a specific dose-response model for the SARS-CoV virus associated with infectious pneumonia.

$$P = 1 - \exp\left(-\frac{d}{k}\right) \quad (3)$$

where d is the number of inhaled virus particles and k is the fit coefficient, which is related to the virus' characteristics. For the SARS-CoV virus, Watanabe used the $k = 4.1 \times 10^2$ (PFU) exponential model as the dose-response model for this virus. Where PFU (Plaque Forming Unit) is a unit used to measure viral activity. It is a method of determining the concentration of a virus by making a limiting dilution of the virus, inoculating it into a cell culture, forming an area of viral infection on an agar plate, and counting the forming units. Because the volume and morphology of viruses may vary, it may not be accurate to measure the mass or volume of the virus, while PFU is a relatively accurate measure of viral activity. Sampath et al. (2005) analyzed SARS-CoV viruses by PCR and found that for SARS-CoV viruses, there are about 300 retroviral genomes per PFU, so it can be assumed that for SARS-CoV virus, an exponential model with $k = 4.1 \times 10^2 \times 300 = 1.23 \times 10^4$ can be used to predict the probability of infection of SARS pneumonia. d is estimated in relation to the deposition rate of particulate matter in the lungs, the aerosol concentration in the exposed space, and whether or not a mask is worn, and the dose d is estimated by

$$d = \sum_i^n \int_{t_0}^t (1 - \alpha) NVC(\tau) f_i d\tau \quad (4)$$

where N is the number of breaths (20 breaths/min), V is the tidal volume, which is related to the height and movement level of the person, C denotes the concentration of particulate matter, α is the filtration efficiency of personal protective equipment (e.g., mask, protective clothing), and f_i is the fractional deposition of particulate matter entering the human lung through breathing in the i interval. The deposition fraction is calculated using a deposition model for pathogenic bioaerosols (Guha et al., 2014).

2.5 Grid independence verification

The model described in Section 2.1 is structured and meshes in a cartesian coordinate system. Since the grid structure as well as the number of meshes have an impact on the simulation accuracy of the flow field, the grid independence of the model was verified with the aim of achieving a certain level of accuracy while minimizing the number of meshes and saving computer resources. For this purpose, the same model was meshed in three different sizes: 132367, 231779, and 521908, and the grid was encrypted at the larger velocity gradients. By comparing the velocity variation in the vertical direction of the inlet and outlet (Fig. 4), it was found that the difference in velocity variation between the 0.23 million and

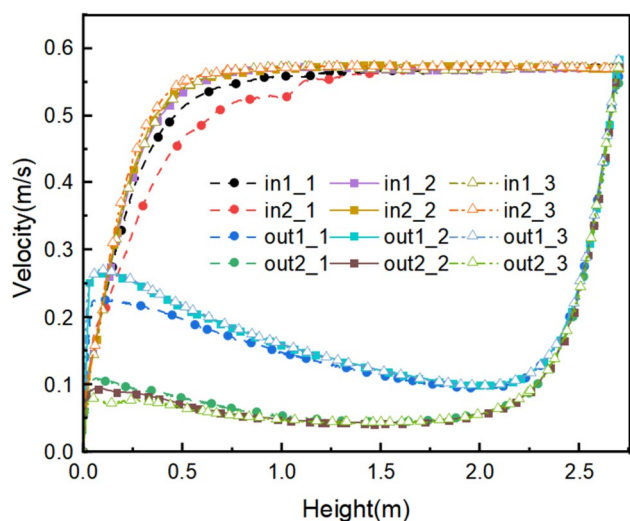


Fig. 4 Sensitivity of velocity to grid for three grids below Inlet and Outlet

0.52 million grids was very small, and therefore the 0.23 million grid size was used as the base model in the subsequent simulations.

3 Results and discussion

3.1 Aerosol distribution in biosafety laboratories

Figure 5a demonstrates the airflow organization in the room, where the upper figure of Fig. 5a shows the

velocity cloud and streamline diagram of the planar flow field at $x=2.075$ m for model one, and the lower figure of Fig. 5a shows the velocity cloud and streamline diagram of the planar flow field at $y=1$ m. From the figure, it can be seen that the streamlines between the air supply and exhaust vents are smoother with fewer eddies, which helps the escape of aerosols, but due to the blocking effect of the personnel, a vortex will be generated in the vicinity of the personnel, which may be unfavorable to the escape of aerosols. Meanwhile, on the far left and right sides of the room, a larger vortex occurs, which is caused by the opposite direction of air-flow in this part of the room to the prevailing airflow, and thus a large number of aerosols can accumulate in these areas. Figure 5b shows the velocity cloud and streamline diagram of the planar flow field for model II. It can be seen that without the obstacles in the way, the flow field produces an additional large vortex at the very bottom. Figure 5b shows the indoor particulate matter distribution over time, with the particle color representing the time the particles are present in the room. It can be seen that under the conditions of this study, the aerosol can fill the whole room within 3 min after leakage and reaches the stabilization between discharge and release (the particles' residence time in the room reaches uniformity) at 6 min. Table 2 demonstrates the variation of aerosol concentration with time. At the beginning of the leak, the aerosol concentration rises rapidly, but after 3 min, the change in aerosol concentration levels off.

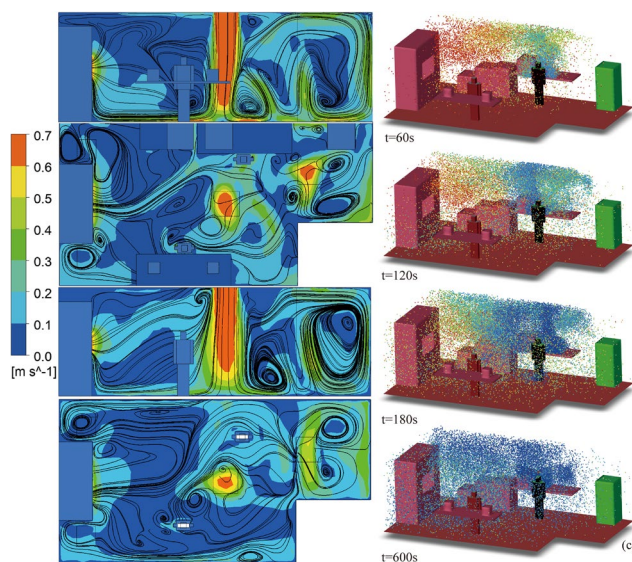


Fig. 5 **a** Velocity contours and streamlines for Model 1 plane $X=2.075$ m and plane $Y=1.5$ m; **b** Velocity contours and streamlines for Model 1; **c** Particle tracks at different times

Table 2 Number and concentration of aerosols at different times in the laboratory

Time(s)	Concentration(article/m ³)	Time(s)	Concentration(article/m ³)
30	163,505.2195	330	785,461.7542
60	274,131.9257	360	800,003.3454
90	357,037.8806	390	807,908.1435
120	445,784.7529	420	813,330.8891
150	515,066.3969	450	816,487.4126
180	577,522.3961	480	818,605.251
210	638,130.3453	510	834,886.9769
240	697,982.8871	540	844,518.4204
270	737,358.4943	570	857,333.3662
300	744,845.1206	600	868,907.2858

3.2 Effect of personal protective equipment on the probability distribution of laboratory infections

The average probability of infection in the laboratory was calculated using the measured response model in Section 2.4 and is shown in Fig. 6. It can be seen that there is a clear hysteresis between the probability of infection and contaminant concentration. The infection probability rises rapidly in the first 6 min and shows an S-shaped curve, with the fastest increase in infection probability at around 2 min and a gradual stabilization after 8 min. In addition, it can be seen numerically that the probability of personnel infection has reached 50% after 200 s after the occurrence of leakage, which implies the importance of leakage detection devices, and the timely detection of pollutant leakage is extremely important for the protection of staff. On the other hand, wearing personal protective devices such as masks can substantially reduce the probability of personnel infection. As can be seen from the red curve, experiencing

the same amount of time, the probability of infection can be reduced by 5 to 10 times under the effect of the mask, with the maximum probability of infection reduced from 94 to 13%. These results demonstrate the importance of personal protective equipment (PPE) in biological laboratories.

3.3 Effect of obstacles and contaminant release locations on the probability distribution of laboratory infections

Figures 7 and 8 respectively present curves depicting the temporal evolution of indoor average aerosol concentration and infection probability under six distinct working conditions. Cases 1–3 correspond to working conditions with obstacles placed transversely, as illustrated in the upper part of Fig. 1, while Cases 4–5 represent working conditions with obstacles positioned longitudinally, as shown in the lower part of Fig. 1. The specific working conditions are detailed in Table 3.

This study compares the impact of different obstacle placements and pollutant release locations on infection rates. As depicted in Fig. 7, environments with obstacles placed laterally exhibit lower indoor pollutant concentrations compared to those with obstacles placed longitudinally. Table 4 reveals that, corresponding to the pollutant source locations, the average concentrations in all scenarios with lateral obstacle placement are lower than those with longitudinal obstacle placement. Furthermore, when the pollutant source is positioned below the exhaust outlet, the average pollutant concentration in scenarios with lateral obstacle placement is approximately 75% less than that in scenarios with longitudinal obstacle placement. Conversely, when the pollutant source is on the tabletop, the average pollutant concentration in scenarios with lateral obstacle placement is only 50% of that in scenarios

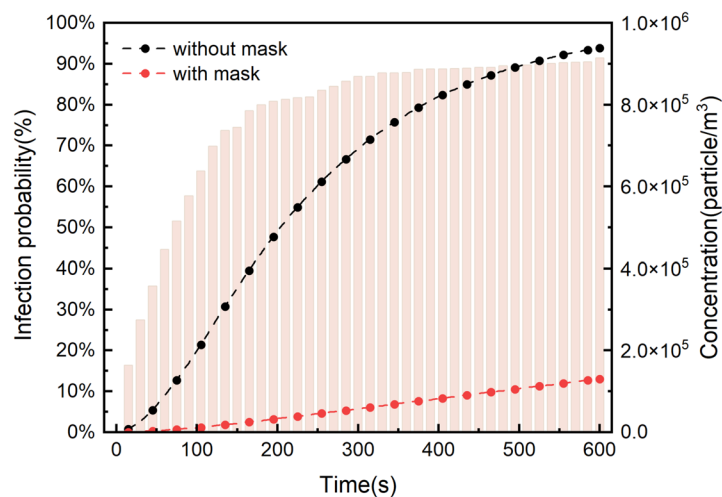


Fig. 6 Particle concentration, infection probability over time

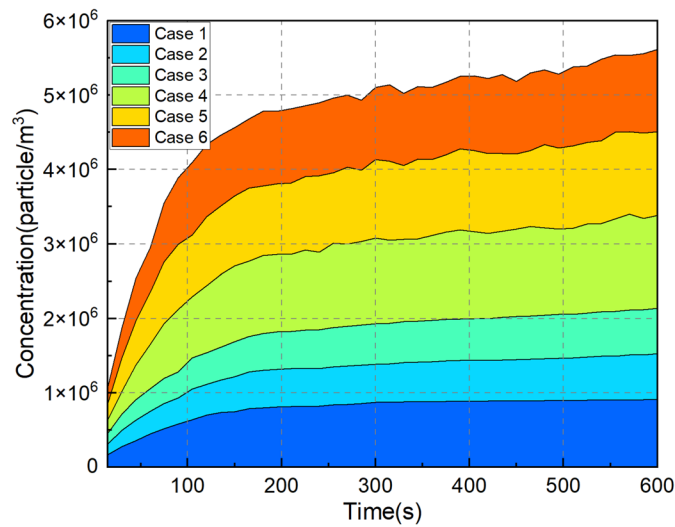


Fig. 7 Variation of concentration under different working conditions

Table 3 Details of working conditions

Case	Obstacle	Source Position
Case 1	Transversely	Source 3
Case 2	Transversely	Source 2
Case 3	Transversely	Source 1
Case 4	Longitudinally	Source 3
Case 5	Longitudinally	Source 2
Case 6	Longitudinally	Source 1

with longitudinal obstacle placement. We hypothesize that this is attributed to the guiding effect of obstacles, which accelerates the emission of pollutants.

Therefore, in summary, in order to effectively reduce the probability of infection in the laboratory, the layout of the laboratory should be reasonably arranged to form

a good inflow area, and try to avoid placing devices containing pollutants near the air supply (Fig. 8).

4 Conclusion

This study analyzed the aerosol distribution of a laboratory spill dealing with the SARS-CoV-2 virus using a CFD approach and predicted the probability of infection using a stoichiometric response model. The study explored the risk of exposure in biosafety laboratories from two perspectives: location of the barrier and location of the leak origin. The key findings of this study are as follows:

- (1) The average indoor pollutant concentration reaches a high level within 3 min of a spill and the probability of infection reaches 50%, and when people remain in a contaminated state, the probability of infection reaches nearly 100% in about 10 min.

Table 4 Variation of concentration under different working conditions

Time(s)	Case 1	Case 2	Case 3	Case 4	Case 5	Case 6
60	445,784.75	303,889.6	305,252	597,266.7	698,326	603,071.1
120	697,982.89	417,578.4	422,070.4	902,908.5	921,458.2	969,774.5
180	800,003.35	504,463.7	492,754.9	1,047,579	934,102.3	1,002,389
240	818,605.25	509,805.5	517,899.2	1,038,235	1,031,830	983,483.7
300	868,907.29	515,835.3	542,692.7	1,149,698	1,057,346	971,394
360	879,091.8	540,399.5	555,683	1,134,136	1,027,160	964,345.5
420	887,765.49	545,242.2	566,663.4	1,139,882	1,075,458	1,008,519
480	895,225.14	565,125.6	586,465.9	1,170,928	1,118,273	1,001,889
540	901,120.01	590,391.3	595,787.1	1,183,853	1,114,753	1,097,023
600	914,029.38	612,810.7	607,536.3	1,247,295	1,128,772	1,101,999

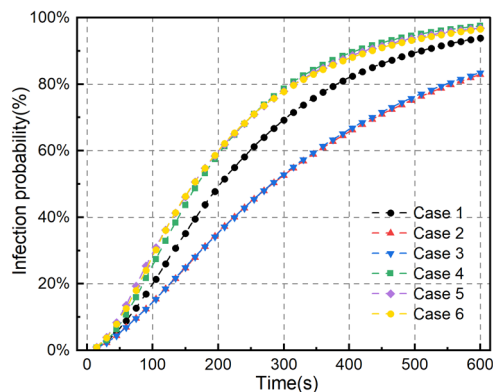


Fig. 8 Probability of infection under different working conditions

- (2) Personal protective equipment such as masks play a very important role in avoiding infection. Wearing a mask can reduce the risk of infection by 5 to 10 times, and in this study, the maximum probability of infection was reduced from 94 to 13%.
- (3) Room layout is extremely important in reducing the concentration of pollutants. Reasonable layout can effectively reduce the probability of infection. Compared with the working condition without obstacles, the working condition with obstacles can reduce the pollutant concentration to 25%~40%.
- (4) The location of the pollution source has a great influence on the increase rate of infection probability. Pollutants far away from the windward side spread more slowly, resulting in a lower probability of infection.

Acknowledgements

This research did not receive any specific grant from funding agencies in the public, commercial, or not-for-profit sectors.

Authors' contributions

Hu Gao: Writing – original draft, Visualization, Validation, Methodology, Software, Investigation, Formal analysis, Data curation. Jing Liu: Writing – review & editing, Supervision, Funding acquisition, Conceptualization, Resources, Project administration.

Availability of data and materials

No data was used for the research described in the article.

Declarations

Competing interests

The authors declare that they have no known competing financial interests or personal relationships that could have appeared to influence the work reported in this paper.

References

- Guha, S., Hariharan, P., & Myers, M. R. (2014). Enhancement of ICRP's lung deposition model for pathogenic bioaerosols. *Aerosol Science and Technology*, 48(12), 1226–1235.
- Huang, J., Hao, T., Liu, X., Jones, P., Ou, C., Liang, W., & Liu, F. (2022). Airborne transmission of the Delta variant of SARS-CoV-2 in an auditorium. *Building and Environment*, 219, 109212.
- Lee, C., Jang, E. J., Kwon, D., Choi, H., Park, J. W., & Bae, G.-R. (2016). Laboratory-acquired dengue virus infection by needlestick injury: A case report, South Korea, 2014. *Annals of Occupational and Environmental Medicine*, 28, 1–8.
- Lim, P. L., Kurup, A., Gopalakrishna, G., Chan, K. P., Wong, C. W., Ng, L. C., Se-Thoe, S. Y., Oon, L., Bai, X., & Stanton, L. W. (2004). Laboratory-acquired severe acute respiratory syndrome. *New England Journal of Medicine*, 350(17), 1740–1745.
- Lippi, G., Horvath, A. R., & Adeli, K. (2020). Editorial and executive summary: IFCC interim guidelines on clinical laboratory testing during the COVID-19 pandemic. *Clinical Chemistry and Laboratory Medicine*, 58(12), 1965.
- Liu, Z., Zhuang, W., Hu, L., Rong, R., Li, J., Ding, W., & Li, N. (2020a). Experimental and numerical study of potential infection risks from exposure to bioaerosols in one BSL-3 laboratory. *Building and Environment*, 179, 106991.
- Liu, Z., Zhuang, W., Hu, X., Zhao, Z., Rong, R., Ding, W., Li, J., & Li, N. (2020b). Effect of equipment layout on bioaerosol temporal-spatial distribution and deposition in one BSL-3 laboratory. *Building and Environment*, 181, 107149.
- Naeem, W., Zeb, H., & Rashid, M. I. (2022). Laboratory biosafety measures of SARS-CoV-2 at containment level 2 with particular reference to its more infective variants. *Biosafety and Health*, 4(1), 11–14.
- Nicas, M., Nazaroff, W. W., & Hubbard, A. (2005). Toward understanding the risk of secondary airborne infection: Emission of respirable pathogens. *Journal of Occupational and Environmental Hygiene*, 2(3), 143–154.
- Pedrosa, P. B. S., & Cardoso, T. A. O. (2011). Viral infections in workers in hospital and research laboratory settings: A comparative review of infection modes and respective biosafety aspects. *International Journal of Infectious Diseases*, 15(6), e366–e376.
- Qian, H., Li, Y., Nielsen, P. V., & Huang, X. (2009). Spatial distribution of infection risk of SARS transmission in a hospital ward. *Building and Environment*, 44(8), 1651–1658.
- Sampath, R., Hofstadler, S. A., Blyn, L. B., Eshoo, M. W., Hall, T. A., Massire, C., Levene, H. M., Hannis, J. C., Harrell, P. M., Neuman, B., Buchmeier, M. J., Jiang, Y., Ranken, R., Drader, J. J., Samant, V., Griffey, R. H., McNeil, J. A., Crooke, S. T., & Ecker, D. J. (2005). Rapid identification of emerging pathogens: Coronavirus. *Emerging Infectious Diseases*, 11(3), 373–379.
- Verreault, D., Moineau, S., & Duchaine, C. (2008). Methods for sampling of airborne viruses. *Microbiology and Molecular Biology Reviews*, 72(3), 413–444.
- Watanabe, T., Bertrand, T. A., Weir, M. H., Omura, T., & Haas, C. N. (2010). Development of a dose-response model for SARS coronavirus. *Risk Analysis*, 30(7), 1129–1138.
- Wu, J. T., Leung, K., & Leung, G. M. (2020). Nowcasting and forecasting the potential domestic and international spread of the 2019-nCoV outbreak originating in Wuhan, China: A modelling study. *The Lancet*, 395(10225), 689–697.
- Yin, S., Sze-To, G. N., & Chao, C. Y. H. (2012). Retrospective analysis of multi-drug resistant tuberculosis outbreak during a flight using computational fluid dynamics and infection risk assessment. *Building and Environment*, 47, 50–57.
- Yu, H., & Thé, J. (2016). Validation and optimization of SST k- ω turbulence model for pollutant dispersion within a building array. *Atmospheric Environment*, 145, 225–238. <https://doi.org/10.1016/j.atmosenv.2016.09.043>
- Zhao, B., Zhang, Y., Li, X., Yang, X., & Huang, D. (2004). Comparison of indoor aerosol particle concentration and deposition in different ventilated rooms by numerical method. *Building and Environment*, 39(1), 1–8.

Publisher's Note

Springer Nature remains neutral with regard to jurisdictional claims in published maps and institutional affiliations.

Received: 24 November 2023 Accepted: 26 January 2024

Published online: 26 February 2024